Hindawi
Journal of Nanomaterials
Volume 2017, Article ID 5075326, 12 pages
https://doi.org/10.1155/2017/5075326

Research Article

Heat Treatment Effect on Eu^{3+} Doped TeO_2-BaO-Bi_2O_3 Glass Systems with Ag Nanoparticles

Tomasz Lewandowski,[1] Michał Dembski,[1] Michalina Walas,[1] Marcin Łapiński,[1] Magdalena Narajczyk,[2] Wojciech Sadowski,[1] and Barbara Kościelska[1]

[1]*Department of Solid State Physics, Faculty of Applied Physics and Mathematics, Gdańsk University of Technology, Gabriela Narutowicza 11/12, 80-233 Gdańsk, Poland*
[2]*Laboratory of Electron Microscopy, Faculty of Biology, University of Gdańsk, ul. Wita Stwosza 57/246, 80-952 Gdańsk, Poland*

Correspondence should be addressed to Tomasz Lewandowski; tlewandowski@mif.pg.gda.pl

Received 28 July 2017; Accepted 1 October 2017; Published 30 October 2017

Academic Editor: Xuping Sun

Glass systems of $73TeO_2$-4BaO-$3Bi_2O_3$-$2Eu_2O_3$-xAg (in molar ratio where $x = 0, 1, 2$, and 3) compositions have been successfully synthesized. Silver nanoparticles were obtained with the employment of heat treatment (HT) procedure executed at 350°C. Glass transition temperatures of different compositions have been determined through DSC measurements. XRD results presented characteristic amorphous halo indicating lack of long range order in the samples. FTIR structural studies revealed that glass matrix is mainly composed of TeO_3 and TeO_4 species and is stable after different applied heat treatment times. X-ray photoelectron spectroscopy (XPS) measurements confirmed that in selected samples part of Ag ions changed oxidation state to form Ag^0 species. TEM measurements revealed nanoparticles of size in the range of 20–40 nm. UV-vis absorption results demonstrated characteristic transitions of Eu^{3+} ions. Additionally, UV-vis spectra of samples heat-treated for 6, 12, 24, and 48 hours presented bands related to silver nanoparticles. Photoluminescence (PL) studies have been performed with excitation wavelength of $\lambda_{exc} = 395$ nm. Obtained spectra exhibited peaks due to $^5D_0$-^7F_J (where $J = 2, 3, 4$) and $^5D_1$-^7F_J (where $J = 1, 2, 3$) transitions of Eu^{3+}. Moreover, luminescence measurement indicated enhancement of rare earth ions emissions in several of the annealed samples. Increase of emission intensity of about 35% has been observed.

1. Introduction

Superior properties, for instance, mechanical and thermal stability, high devitrification resistance, and suitable infrared transparency, make tellurite glasses promising materials for variety of applications related to the field of optics, for example, light upconversion materials, lasers, solar cells, or optical amplifiers [1–6]. Additionally, these glasses are suitable for utilization as luminescent materials owing to their low phonon energy (700 cm^{-1}) in comparison to other oxide glasses and wide transmission window. This property leads to minimization of the nonradiative losses. Tellurite glasses also exhibit good solubility of rare earth ions that allows for possible employment of their *f-f* transitions in order to obtain efficient light sources with tunable emission color [7, 8].

In recent years, glasses doped with silver gained much attention considering possibility of the localized surface plasmon resonance (LSPR) phenomenon utilization. LSPR is observed in case of nanoparticles with sizes smaller than 100 nm. Electron excitations creating charge oscillations at the metal-insulator boundary lead to large local electric field enhancement in the vicinity of nanoparticles, creating so called "hot-spots." As a result, it is possible to increase the intensity of rare earth ions emissions. Formation of silver nanoparticles is facilitated by high mobility of silver ions in tellurite glass matrix and suitable redox potential of $Ag^+ \rightarrow Ag^0$ reduction [9]. Silver is reduced through one-step process:

$$Ag^+ + 1e^- \longrightarrow Ag^0 \quad (1)$$

with the reduction potential of $E_0 = 0.7996$ V [10]. Highly mobile silver ions are form nanoparticles by matrix-assisted reduction process, for example, by structural elements of TeO_2 matrix with uncompensated charge. Silver diffuses into tellurite glass matrix, changes its valance state, and forms nanoparticles through Ostwald ripening. Thus, it is promising to synthesize the nanoparticles inside glass matrix and in consequence achieve emission enhancement of rare earth ions with employment of metal nanoparticles.

One of the first reports on LSPR in glass medium was the work of Malta et al. [11] on borosilicate glasses. Enhancement of Eu^{3+} ions emissions has been observed. Lately, numerous works concerning silver nanoparticles and emission enhancements through LSPR phenomenon have been reported in case of various glass systems [12–15]. Number of studies described the formation of silver nanoparticles in glass matrix through heat treatment approach. While in higher temperatures mobility of silver ions increases, heat treatment approach involves annealing of samples usually above glass transition temperature to introduce metallic nanoparticles [16]. That method is widely applied in order to create nanoparticles through their agglomeration and to obtain enhancement of rare earth emission intensity. Jiao et al. examined the luminescence of Eu^{3+} in borate glasses after addition of silver and mechanisms of Ag ions agglomeration. In this case, enhancement of emission intensities has been detected [17]. White light emission in europium doped phosphate glasses was obtained by Fan et al. [18]. In this study, an efficient energy transfer between nanoparticles and Eu^{2+} and Eu^{3+} species has been detected. Moreover, a number of studies were dedicated to describe silver influence on rare earths emission intensities in matrices demonstrating lower phonon energies such as tellurite and tellurite based glasses.

Amjad et al. [19] studied the influence of silver nanoparticles on the luminescence properties of Eu^{3+} in TeO_2-ZnO glass systems and obtained increase of emission intensities of europium ions. Dousti et al. focused on the silver doped TeO_2-PbO glasses [20]. Du et al. reported tellurite-germanate glasses for solar converters doped with Ag nanoparticles to enhance Pr^{3+} emission intensity [21]. Fares et al. obtained TeO_2-BaO-Nb_2O_5-Er_2O_3 glasses with embedded silver nanoparticles [22]. Enhancement of lifetime and emission intensities of the Er^{3+} $^4I_{13/2} \rightarrow {}^4I_{15/2}$ transition has been observed. Huang et al. studied Er^{3+}/Tm^{3+} codoped TeO_2-ZnO-Na_2CO_3-Er_2O_3-Tm_2O_3-$AgNO_3$ glasses doped with silver and observed 1.85 μm band fluorescence enhancement mainly attributed to the intensified local field effect induced by Ag NPs [23]. Wu et al. presented study on influence of silver on Er^{3+}/Yb^{3+} codoped TeO_2-Bi_2O_3-TiO_2 glasses [24].

To the best of our knowledge, there are no reports on europium doped TeO_2-BaO-Bi_2O_3-Ag (TBBAg) systems with silver nanoparticles obtained through heat treatment process. Similar glass materials have never been studied in terms of silver incorporation and its influence on rare earth ions emission. The aim of this work is the synthesis of silver nanoparticles in tellurite glass matrix and to study the influence of silver addition on luminescence of europium ions incorporated into TBBAg glass. This novel glass matrix is promising material for Eu^{3+} host with its excellent properties. Since TeO_2 is conditional glass former, BaO is introduced to stabilize the glass matrix. Heavy metal oxides such as barium oxide are proven to induce higher devitrification resistance of glasses [25]. Moreover, low phonon energy of tellurite glass promotes radiative transitions of rare earth ions. The aforementioned properties of synthesized glass matrix are the reason that it has been used in this work. Silver nanoparticles, on the other hand, are introduced to study the rare earth ions emission enhancement through LSPR phenomenon. It has never been done before in glass system of similar composition. Since this work is also focused on matrix influence on luminescence of rare earth ion, europium ions have been chosen as a luminescent center since its emission properties are well understood. Additionally, study of the LSPR as a function of different amount of silver in glass is performed. Finally, influence of heat treatment procedure on luminescent properties of obtained material is discussed. TBBAg system is promising material for color tunable phosphors that can be used in LEDs and in lighting industry.

2. Experimental

Synthesis of tellurite glass samples involved mixing and pulverizing of high purity TeO_2, $BaCO_3$, $Bi_5O(OH)_9(NO_3)_4$, $Eu(NO_3)_3$, and $AgNO_3$ raw materials in powder form. Conventional melt-quenching technique has been used to obtain amorphous glass material. Well-mixed batches were placed in porcelain crucibles and were gradually heated to 800°C in order to enhance the mixing of ingredients. After 30 minutes the temperature was reduced to 700°C for the next 30 minutes. Afterwards, obtained melt was poured onto a preheated steel plate (300°C), pressed immediately between steel plates, and then cooled down to room temperature. Each stage of this procedure was carried out in the air atmosphere. Such approach led to synthesis of homogenous, transparent samples.

Heat treatment (HT) stage involves annealing of the samples usually above glass transition temperature. In this work, heat treatment at 350°C in the air atmosphere has been applied. This has been done to initiate the migration of silver ions that would lead to formation of silver nanoparticles embedded in glass matrix. HT procedure is considered to be the method of choice in case of solid state samples since it is a simple, one-step process that allows controlling annealing parameters. Different HT times have been applied in order to study the evolution of the glass system and change of sample properties. HT parameters are presented in Table 1 in detail.

Differential scanning calorimetry (DSC) measurements were executed on Netzsch Simultaneous TGA-DSC, STA 449 F1, in order to determine the thermal properties of the material such as glass transition and crystallization temperature. Investigations were conducted on powder samples in platinum-rhodium crucibles with heating rate of 15°C min^{-1} in the air atmosphere. Structural investigations were performed using several techniques. Examination of internal structure of prepared samples was carried out using

Table 1: Parameters of heat treatment performed on obtained samples.

Sample series	Composition (molar ratio)	HT (h)	T (°C)
Ag0	$73TeO_2$-4BaO-$3Bi_2O_3$	—	—
Ag1	$73TeO_2$-4BaO-$3Bi_2O_3$-1Ag	0, 3, 6, 12, 24, 48, 96	350
Ag2	$73TeO_2$-4BaO-$3Bi_2O_3$-2Ag	0, 3, 6, 12, 24, 48, 96	
Ag3	$73TeO_2$-4BaO-$3Bi_2O_3$-3Ag	0, 3, 6, 12, 24, 48, 96	
AgEu1	$73TeO_2$-4BaO-$3Bi_2O_3$-$2Eu_2O_3$-1Ag	0, 3, 6, 12, 24	
AgEu2	$73TeO_2$-4BaO-$3Bi_2O_3$-$2Eu_2O_3$-2Ag	0, 3, 6, 12, 24	
AgEu3	$73TeO_2$-4BaO-$3Bi_2O_3$-$2Eu_2O_3$-3Ag	0, 3, 6, 12, 24	

conventional X-ray diffraction (XRD) technique. Measurements were executed on powder samples using Philips X'PERT PLUS diffractometer with Cu-Kα radiation (λ = 0.154 nm). Chemical bonds existing in the structural units of the glass samples were determined using Fourier Transform Infrared (FTIR) spectroscopy results. These measurements were undertaken on Perkin-Elmer Frontier MIR/FIR spectrometer with TGS detector in the midinfrared spectral range. Examination involved creating pellet-type samples containing mixture of glass with potassium bromide (KBr) in weight ratio 1 : 100. The same amount of ingredients with controlled grain size was introduced in case of all measured samples. Measurements were performed with 0.5 cm^{-1} spectral resolution. X-ray photoelectron spectroscopy analysis (XPS) was carried out with the employment of X-ray photoelectron spectrometer (Omicron NanoTechnology) with 128-channel collector. Investigated samples were precleaned by Ar ion beam. XPS measurement has been done at room temperature in ultrahigh vacuum conditions, below 1.1×10^{-8} mBar. The photoelectrons were excited by an Mg-Kα X-ray source. The X-ray anode was operated at 15 keV and 300 W. Omicron Argus hemispherical electron analyser with round aperture of 4 mm was used for analysing of emitted photoelectrons. The binding energies were corrected using the background C1s line (285.0 eV) as a reference. XPS spectra were analysed with Casa-XPS software using a Shirley background subtraction and Gaussian–Lorentzian curve as a fitting algorithm. For transmission electron microscopy TEM samples were placed on copper grids coated with a 2% collodion solution and carbon. Probes were examined using a Tecnai Spirit BioTwin (FEI) electron microscope at 120 kV. UV-vis spectra were collected on Perkin-Elmer Lambda 35 UV-vis spectrophotometer in the range of 350–700 nm. Measurements were conducted in the air atmosphere. Photoluminescence (PL) spectra were collected in the 430–750 nm range in case of emission spectra and 250–500 nm for excitation spectra using Perkin-Elmer LS 55 spectrofluorometer. Measurements were performed using pellet samples mixed with KBr in weight ratio of 1 : 1.

Calculations of the extinction coefficients were achieved using the multireflectance formula [27]:

$$T = \frac{(1-R)^2 \times e^{-\alpha d}}{\left((1-R)^2 \times e^{-2\alpha d}\right)}, \quad (2)$$

where α is the extinction coefficient, d is the sample thickness, R is the reflectance, and T is the transmittance. For each sample, values of reflectance and the transmittance were measured. Extinction coefficient value was calculated by subtracting the extinction coefficient of the sample without silver addition from that of the annealed samples containing silver nanoparticles.

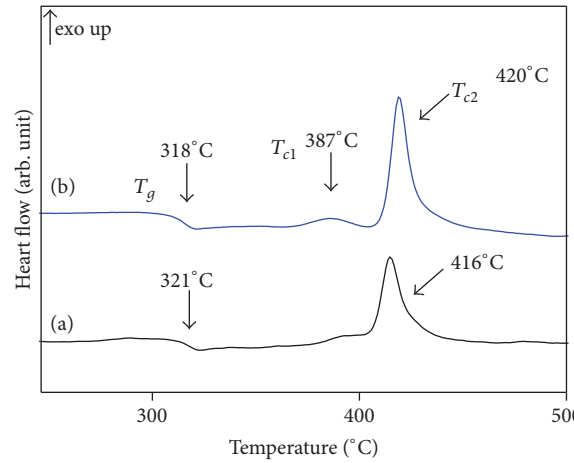

Figure 1: DSC spectrum of Ag0 (a) and Ag1 (b) glass samples.

Table 2: Thermal parameters of Ag0 and Ag1 glass samples.

Sample	T_g (°C)	T_{c1} (°C)	T_{c2} (°C)	TS (°C)
Ag0	321	—	416	95
Ag1	318	387	420	69

3. Results and Discussion

3.1. Structural Studies

3.1.1. DSC. DSC curves of Ag0 and Ag1 glass samples are presented in Figure 1((a) and (b)). Glass transition temperature T_g is located at 321 and 318°C, respectively. In case of Ag0 sample, one clear exothermic peak attributed to the crystallization process may be distinguished at 416°C. On the other hand, DSC curve of Ag1 consists of the main crystallization peak at 420°C and, additionally, another exothermal peak at 387°C. Thermal stability [28] (TS) regions have been determined and equaled 95°C in case of Ag0 and 69°C for Ag1 sample. Thermal parameters of studied samples are presented in Table 2.

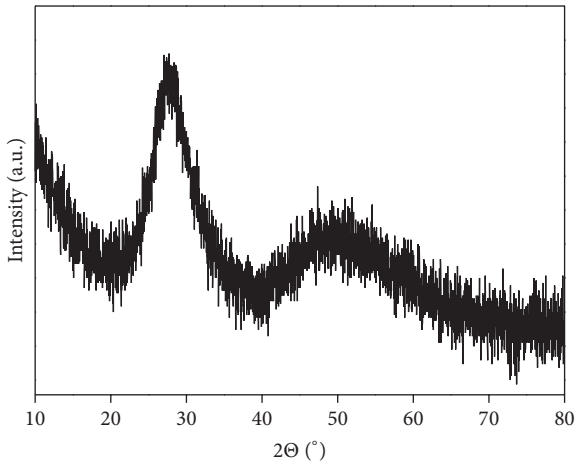

Figure 2: XRD result of AgEu1 glass sample annealed for 6 hours.

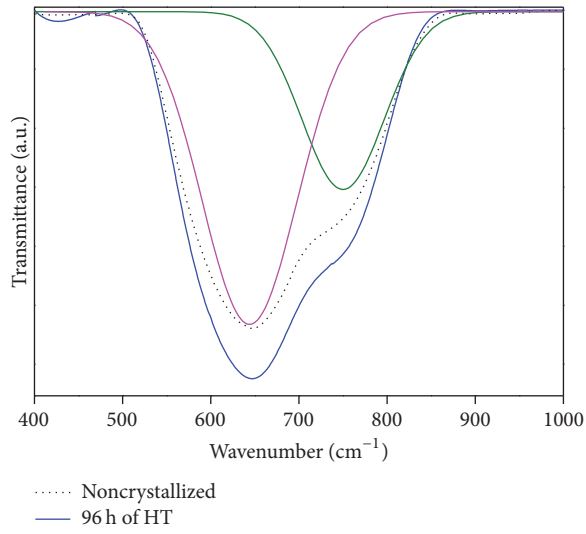

Figure 3: FTIR spectrum of Ag1 sample noncrystallized (dotted line) and heat-treated for 96 h (solid line). The pink curve refers to signal due to vibrations in TeO_4 elements while the green one refers to vibration signal in TeO_3.

These measurements have been performed mainly in order to investigate the TS region. Its range is crucial for silver nanoparticles formation process, considering the fact that their synthesis is usually performed below the temperature of the first crystallization peak but above the glass transition temperature. Above T_g, glass properties such as viscosity and ion mobility change, favoring silver nanoparticles agglomeration. Additionally, such approach prevents the crystallization of glass matrix which is the case in our work.

Therefore, synthesis of Ag nanoparticles has been performed in the range between T_g and the onset of the first crystallization peak at 387°C. It is our consideration that used temperature range would be sufficient to initialize migration of silver ions to form silver nanoclusters. This is possible due to decrease of glass viscosity with increasing temperature.

3.1.2. XRD. XRD results were obtained for glass materials annealed for 3, 6, 12, and 24 hours. Amorphous halo is evident indicating that no long range order periodicity existed in the samples. It was not possible to detect any Ag nanoparticles signals, because only 1–3 mol% of silver was introduced into the samples.

On the other hand, in case of nanoparticles one can observe widening of diffraction peaks and due to nanoscale size such peak can overlap with wide amorphous halo. Exemplary result of AgEu1 sample heat-treated for 6 hours is presented in Figure 2.

3.1.3. FTIR. FTIR technique was employed to reveal any structural alterations induced by heat treatment procedure or by the change of composition. Moreover, basic structural elements of the matrix were also revealed. Tellurite glasses are usually composed of TeO_3 pyramids and TeO_4 trigonal bipyramids. Obtained measurement results of as-prepared and heat-treated Ag1 samples are presented in Figure 3. To examine heat treatment induced changes in tellurite glass matrix two samples have been chosen for measurement: as-prepared and heat-treated for 96 hours. Main feature is the wide band visible in the 530–850 cm^{-1} range. This band can be deconvoluted into two signals positioned at 650 cm^{-1} and 730 cm^{-1}. The first one (pink curve) at 650 cm^{-1} came from Te-O stretching vibrations of TeO_4 trigonal bipyramids [29–31]. The second one (green curve) at approximately 730 cm^{-1} is associated with oscillations of Te-O in TeO_3 trigonal pyramids [30, 31]. TeO_4 derived signal is stronger in both cases. This might indicate that more TeO_4 species exist in obtained material.

Intensities of the aforementioned bands varied slightly as a function of annealing time. Heat treatment for 96 h resulted in increased intensity of these two peaks. However, observed changes of FTIR spectra are minor. Ratio between intensities of TeO_4 and TeO_3 derived bands remained approximately constant. Therefore, it is concluded that glass matrix is resistant to heat treatment procedure and stays unchanged even when long annealing times have been applied. It is consistent with XRD results that indicated no crystallization of glass matrix after HT process.

3.1.4. XPS. XPS experiment has been performed to provide insight on valance state of silver in tellurite glass matrix. Exemplary spectra of as-prepared Ag1 sample, Ag1, and Ag3 samples crystallized for 6 h are presented in Figure 4(a). $Ag3d_{5/2}$ and $Ag3d_{3/2}$ photoelectron peaks of silver have been observed at 368 and 374 eV, respectively. Spin orbit components in all cases were separated by distance of 6 eV which is characteristic of silver. Shape of obtained spectra is comparable to others published before [32]. However, it is difficult to distinguish between different silver state components of $3d_{5/2}$ peak. Therefore, definition of silver oxidation state on the basis of XPS measurements is challenging and sometimes impossible. Consequently, modified Auger parameter (α') had to be calculated. In order to acquire it, kinetic energy values of silver M4VV Auger lines are determined (presented in Figure 4(b)). Their positions equaled 355.6 eV, 357.3 eV, and 357.6 eV in case of Ag1 (HT = 0 h), Ag1 (HT = 6 h), and

Table 3: Results of XPS measurement performed on Ag1 and Ag3 glass samples.

Sample	HT (h)	$Ag3d_{5/2}$ (eV)	$Ag3d_{3/2}$ (eV)	M4VV (eV)	α' (eV)
Ag1	0	368.0	374.2	355.6	723.6
Ag1	6	368.1	373.9	357.3	725.4
Ag3	6	368.0	374.0	357.6	725.6
Value of Auger parameter of metallic silver [26]:					726.0

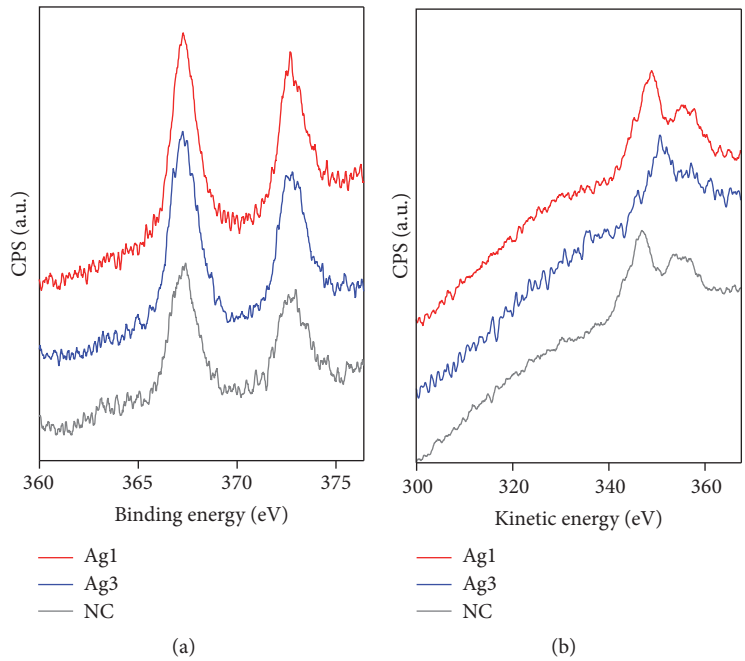

Figure 4: Ag3d photoelectron peaks (a) and Auger lines (b) of Ag1 and Ag3 heat-treated samples and noncrystallized (NC) Ag1 sample.

Ag3 (HT = 6 h) samples, respectively. Parameter has been calculated according to the following equation:

$$\alpha' = \mathrm{BE}\left(\mathrm{Ag3d_{5/2}}\right) + \mathrm{KE}\left(\mathrm{Ag\ M4VV}\right), \quad (3)$$

where $\mathrm{BE}(\mathrm{Ag3d_{5/2}})$ is the binding energy of $\mathrm{Ag3d_{5/2}}$ peak and KE(Ag M4VV) is kinetic energy of M4VV Auger line peak. Parameter α' for metallic silver equals 726 eV [26]. Calculated results are presented in Table 3.

As-prepared Ag1 sample possessed lowest modified Auger parameter which suggests that in case of Ag1 specimen most of silver exists in ionic form. It is indicative that mixture of metallic and ionic silver exists in both heat-treated samples since obtained results are in the range between parameters characteristic to AgO species and metallic silver.

However, some portion of silver ions changed their valance state and formed Ag^0 species. For heat-treated Ag1 sample parameter α' equaled 725.4 eV which means that mixture of Ag oxidation states existed with the great majority of Ag^0 species. Moreover, parameter of Ag3 sample is even higher and equals 725.6 which confirms that most of silver exists in Ag^0 form. Since the value of parameter for Ag3 sample is close to that of metallic silver, it is concluded that ratio of Ag^0 to other Ag species in that specimen is the highest of all samples.

Additional study has been performed on Ag1 sample heat-treated for 6 hours in order to describe bismuth ions valance state. There was a possibility of bismuth reduction and nucleation since heat treatment process created environment propitious for metallic nanoparticles formation. No evidence for bismuth nucleation has been obtained since bismuth Bi4f signals observed (Figure 5) are characteristic to bismuth in oxide state. Peaks possess symmetric shape and are positioned at 159.6 and 164.9 eV (for $\mathrm{Bi4f_{7/2}}$ and $\mathrm{Bi4f_{5/2}}$, resp.). Thus, it can be concluded that only Bi^{3+} ions exist in glass matrix. This is consistent with the fact that Bi_2O_3 is conditional glass former and probably is one of the components creating the amorphous matrix.

3.1.5. TEM. In order to observe the silver nanoparticles embedded in tellurite glass material, TEM measurement has been performed. Samples with Ag1, Ag2, and Ag3 designations annealed for 6 hours has been chosen for measurement. Exemplary TEM images have been presented in Figures 6(a), 6(b), and 6(c). As it can be noticed, nanoparticles are indeed synthesized within amorphous tellurite glass matrix. The shape of nanoparticles is spherical. However, nanoparticles of different size have been obtained in different samples. Increase of dimensions with increasing amount of introduced silver can be observed. In case of Ag1 samples nanoparticles

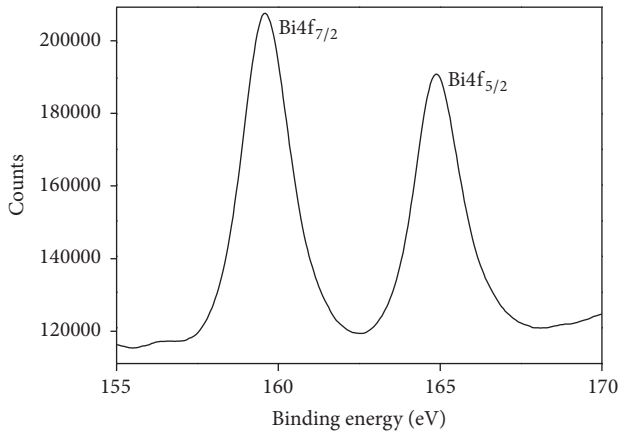

Figure 5: Bi4f photoelectron peaks in Ag1 sample heat-treated for 6 h.

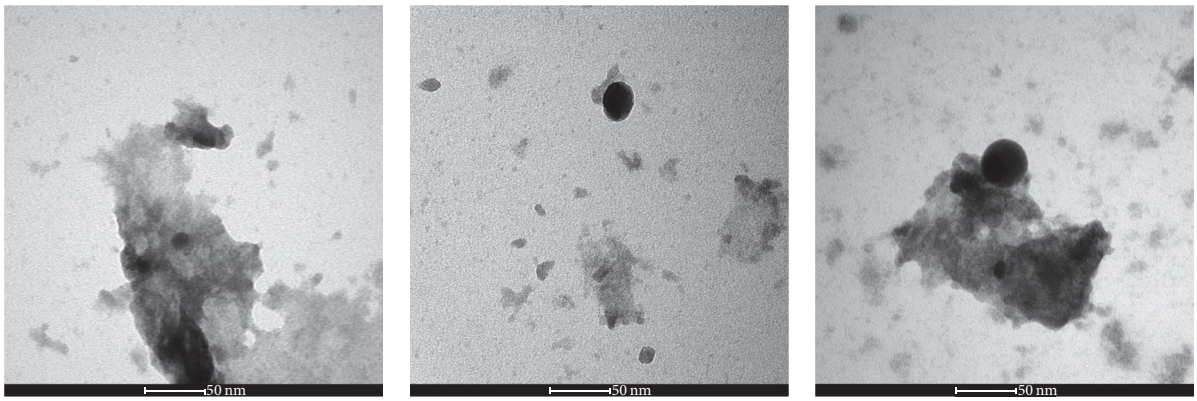

(a) (b) (c)

Figure 6: TEM images of Ag1, Ag2, and Ag3 samples heat-treated for 6 hours ((a), (b), and (c), resp.).

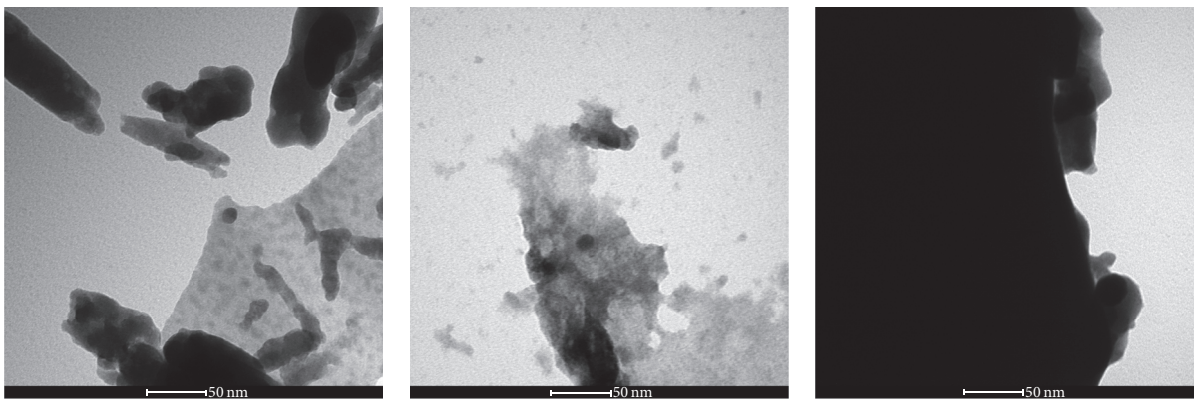

(a) (b) (c)

Figure 7: TEM images of Ag1 samples heat-treated for 3, 6, and 12 hours ((a), (b), and (c), resp.).

size does not exceed 30 nm whereas in Ag2 and Ag3 sample sizes exceed 30 nm and 40 nm, respectively.

TEM measurements are strongly supported with the aforementioned XPS results which indicated that majority of silver is in metallic form in Ag3 sample. Increased number of Ag^0 species resulted in formation of larger agglomerates.

In Figure 7 exemplary TEM images of Ag1 samples heat-treated for 3, 6, and 12 hours have been presented. It is worth noticing that with changing heat treatment time diameter of observed nanoparticles increases with heat treatment duration. In samples heat-treated for 3 hours nanoparticles are not exceeding 20 nm in diameter. On the other hand in

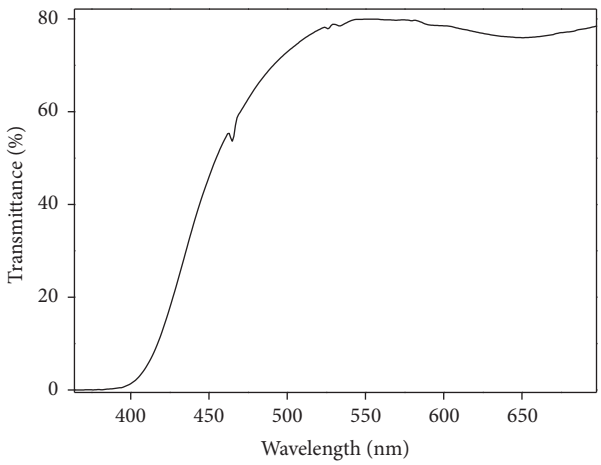

Figure 8: UV-vis transmittance spectrum of AgEu1 sample.

sample heat-treated for 12 hours nanoparticles of 30–40 nm have been observed. It can be thus concluded that change of heat treatment parameters influences the size of silver nanoparticles embedded in tellurite glass matrix.

3.2. Optical Studies

3.2.1. UV-vis. UV-vis spectrum of AgEu1 sample is shown in Figure 8. It can be noticed that absorption signals characteristic to Eu^{3+} were present. Peaks at 465 and 532 nm due to $^7F_0$-$^5D_2$ and $^7F_0$-$^5D_1$ transitions have been observed and assigned on the basis of the energy levels reported in [33].

To observe the influence of Ag quantity on silver nanoparticles formation samples without europium addition have been measured first. In Figures 9(a), 9(b), and 9(c) extinction coefficient in function of wavelength has been presented for obtained series. Through application of different HT conditions, it is possible to obtain tunable LSPR peak depending on silver content. Position and intensity of LSPR band varied slightly with different HT time applied. Samples heat-treated for 6, 24, and 48 hours are shown. Moreover, amount of incorporated silver is also a factor influencing the LSPR band intensity and position. It might indicate that silver nanoparticles size can be altered through change of silver content and performing different HT procedure. However, due to the fact that observed LSPR bands are very wide and amount of introduced silver is small it is difficult to accurately calculate exact shift value of LSPR bands caused by the changes of nanoparticle sizes.

Surface plasmon band is visible in Figures 9(a), 9(b), and 9(c) in the range of 500–550 nm. Silver LSPR peak has been observed above 500 nm in [22, 34]. In tellurite matrix with its refractive index of approximately 2, LSPR band shifts to higher wavelengths in comparison to silicate glasses [20]. This is consistent with the following equation [35]:

$$\lambda_{\max}^2 = \frac{2\pi cmNe^2\left(\varepsilon_\infty + 2n^2\right)}{\varepsilon_0}, \quad (4)$$

where N is the concentration of free electrons, ε_∞ is the metal optical dielectric function, ε_0 is the permeability of free space, n is the refractive index of glass host, and c and m are speed of light and electron effective mass, respectively. One can find that wavelength of LSPR depends on refractive index of glass matrix. Thus, LSPR is red shifted in case of matrices with higher refractive indices [36].

UV-vis results are consistent with XPS and TEM measurements presented in previous section. Observation suggests the successful nanoparticles formation.

3.2.2. Photoluminescence. In case of excitation spectrum monitored at 615 nm, several bands corresponding to the 4*f*-4*f* transitions of Eu^{3+} are apparent. They were assigned to $^7F_0$-$^5D_4$ (362 nm), $^7F_0$-$^5L_7$ (382 nm), $^7F_0$-$^5L_6$ (395 nm), $^7F_1$-$^5D_3$ (415 nm), and $^7F_0$-$^5D_2$ (465 nm) transitions [19, 37]. Spectrum of AgEu1 sample is presented in Figure 10.

In case of 395 nm excitation, number of peaks due to transitions of Eu^{3+} was observed. Starting with low wavelengths, signals at 536 and 557 nm (as a result of $^5D_1$-$^7F_1$ and $^5D_1$-$^7F_2$, transitions) and peaks at 588, 615, 654, and 703 nm ($^5D_0$-$^7F_1$, $^7F_2$, $^7F_3$, and $^7F_4$ transitions) can be noticed [37–40]. Additionally, matrix spectrum (Ag0 sample) has been obtained as a reference which is included in presented emission spectra.

The same excitation has been used for samples with silver nanoparticles generated through heat treatment process. Results are presented in Figures 11(a), 11(b), and 11(c). For AgEu1 sample annealed for 3, 6, and 12 hours increase of Eu^{3+} emission intensities was observed. Maximum of $^5D_0$-$^7F_2$ band intensity (615 nm) was detected for 6 hours of HT time. This can be explained by LSPR which enhances europium ions transitions. Eu^{3+} ions lying near silver nanoparticles are influenced by increased local field around AgNPs. Radiative transition of $^5D_0$-$^7F_2$ is electric-dipole transition [41]. It is hypersensitive to local environment change and modification of local symmetry. Considering this, increase of its intensity may indicate influence of silver nanoparticles. Ratio between intensities of $^5D_0$-$^7F_2$ peak and $^5D_0$-$^7F_1$ magnetic-dipole transition (588 nm) allows evaluating if the intensity change of $^5D_0$-$^7F_2$ transition has the origin in electric field enhancement. This parameter reached the maximum of its value after HT of 6 hours. This is indicative for local electric field influence of AgNPs. To visualize interaction between rare earth ions and silver nanoparticles energy level diagram of Eu^{3+} has been presented in Figure 12.

However, when longer heat treatment times have been applied, quenching of europium transitions was noticed. It is apparent in case of emission spectrum of the AgEu1 sample annealed for 24 hours. This is most likely caused by Eu^{3+}-AgNP energy transfer processes that hinder the radiative transitions of Eu^{3+} and promote nonradiative relaxations. Additionally, growth of silver nanoparticles could lead to decrease of Eu^{3+}-AgNP distance that enhances energy transfer processes [42]. At shorter Eu^{3+}-AgNP distance dipole-dipole interactions become significant resulting in decrease of europium ions luminescence intensity [43, 44]. Quenching

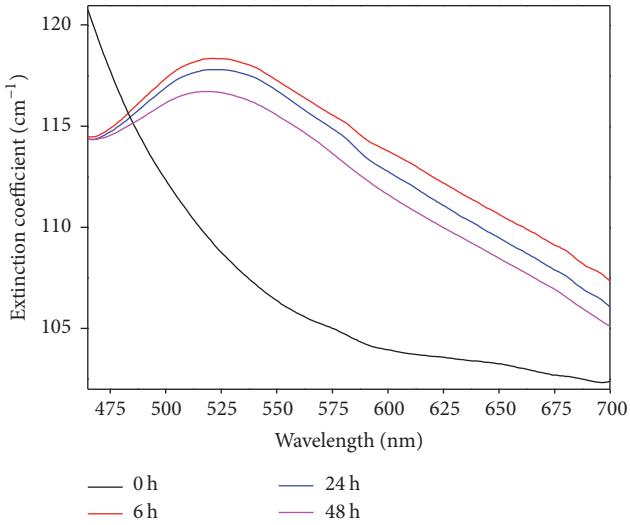

(a) LSPR band in Ag1 series

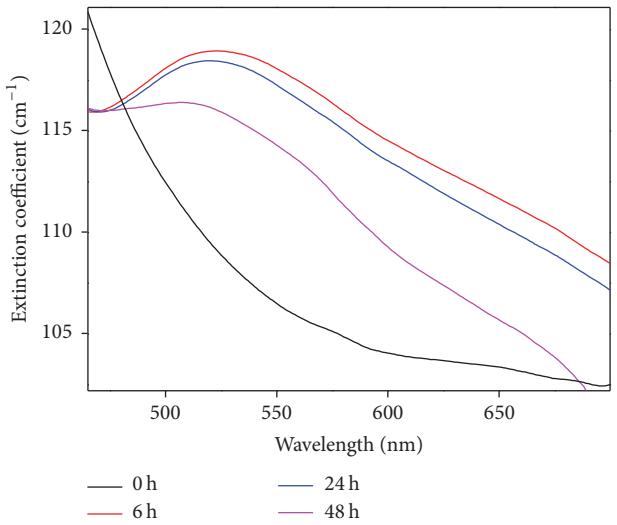

(b) LSPR band in Ag2 series

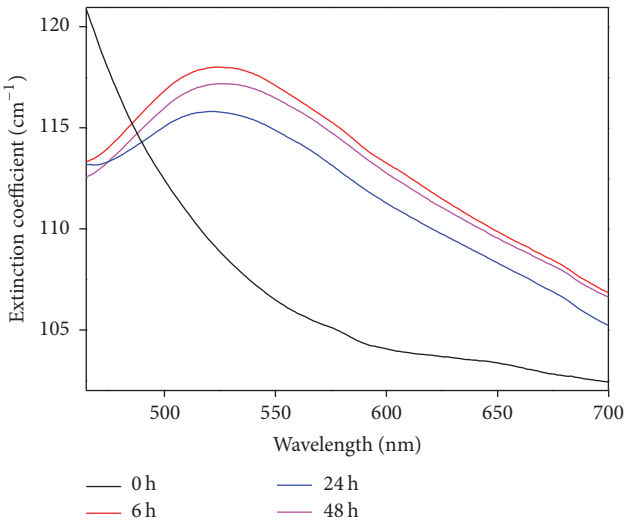

(c) LSPR band in Ag3 series

Figure 9

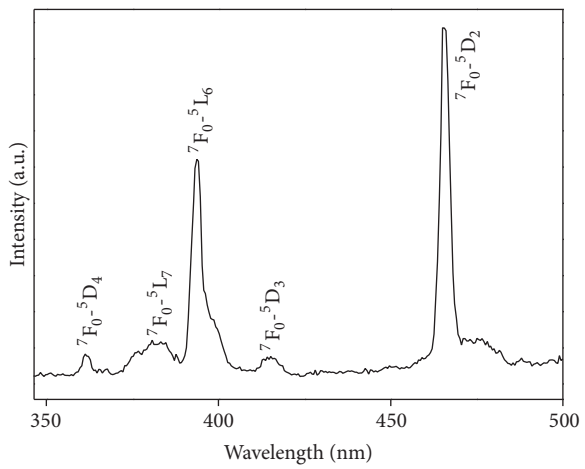

Figure 10: Excitation spectrum of AgEu1 glass sample with λ_{em} = 615 nm.

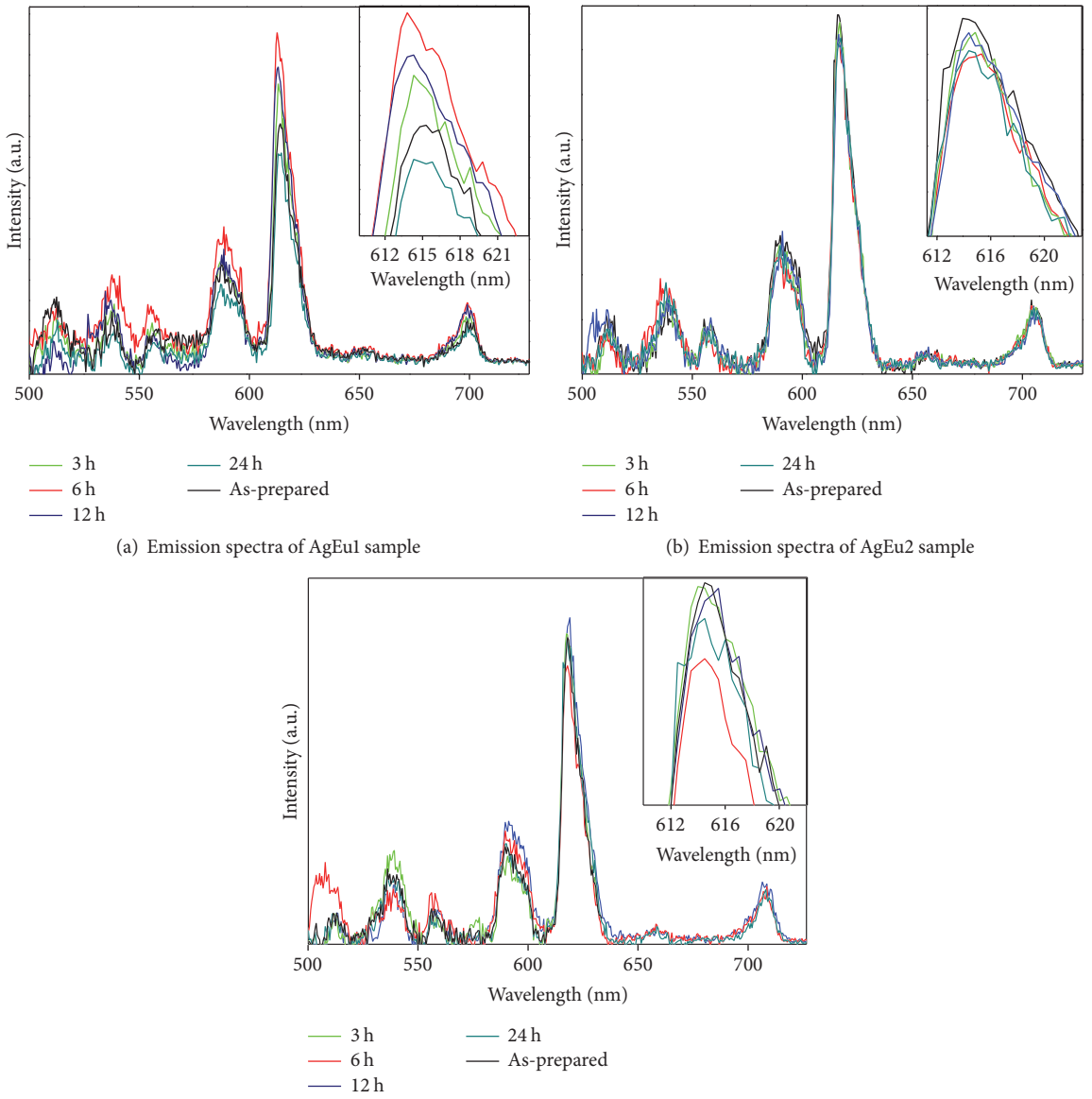

(a) Emission spectra of AgEu1 sample

(b) Emission spectra of AgEu2 sample

(c) Emission spectra of AgEu3 sample

Figure 11

can also have its origin in increased absorbance of silver nanoparticles grown for longer time periods.

For AgEu2 and AgEu3 glass samples, enhancement of europium emission bands is not observed. The reason is probably an excessive amount of silver added to glass sample. Quenching can occur when ratio of RE ions to silver is below one. Energy transfer mechanisms such as $Eu^{3+} \rightarrow$ AgNP transfer takes place which ultimately prevents the increase of europium ions emission intensities [9, 45]. It should be noted that relative position between AgNPs and Eu^{3+} ions is crucial since dipole interactions dominate over local field enhancement when distance separating them becomes shorter. Due to possible small separation between ions and nanoparticles this quenching mechanism cannot be neglected.

Observed lack of enhancement in case of Ag2 and Ag3 series is consistent with TEM results. At higher concentrations silver creates larger agglomerates which could be observed in Figure 6. In case of those samples size of the nanoparticles is not optimal for emission enhancement of rare earth ions. At this point, energy transfer mechanisms become dominant. Moreover, absorption of silver nanoparticles may have increased with size and as a result intensity of rare earth ions emission is decreased. In our system, silver nanoparticles of sizes exceeding approximately 30 nm resulted in lack of Eu^{3+} luminescence enhancement. It is thus concluded that dimensions of silver nanoparticles should be strictly controlled in order to avoid quenching in compositions with higher silver content. This could be

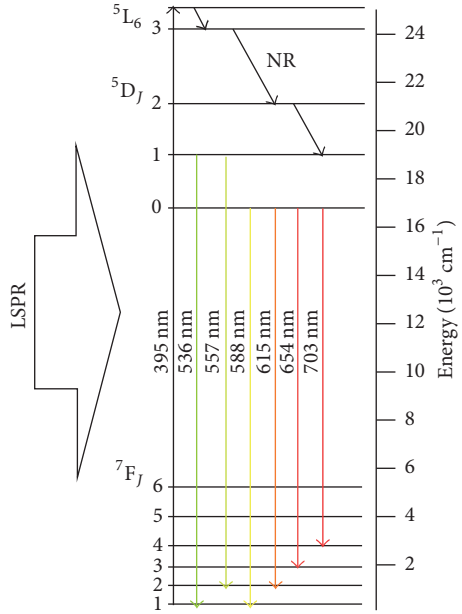

FIGURE 12: Energy level diagram of Eu^{3+} ions. Observed emissions represented by lines of different colors.

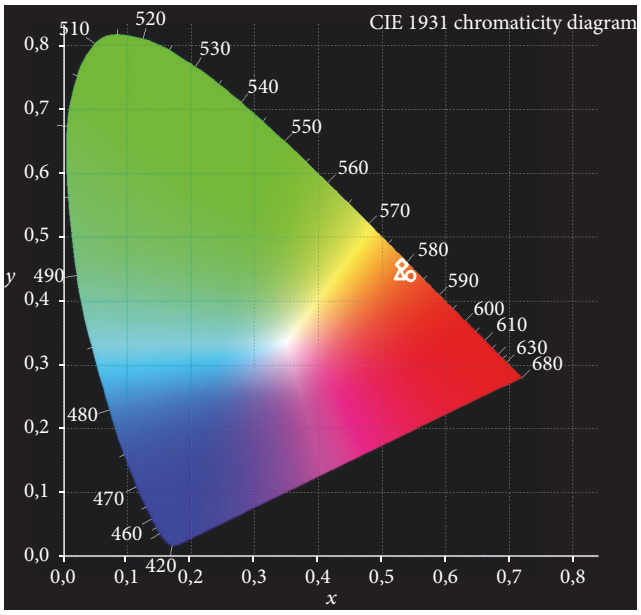

FIGURE 13: CIE chromaticity diagram of AgEu1 (diamond), AgEu2 (circle), and AgEu3 (triangle) samples heat-treated for 6 hours.

done with introduction of appropriate silver amount and heat treatment time. In case of this work, best results were obtained in samples with silver nanoparticles of sizes below 30 nm. Such nanoparticles have been synthesized in AgEu1 series heat-treated for 6 hours.

Exemplary CIE diagrams of Ag1, Ag2, and Ag3 samples heat-treated for 6 hours are presented in Figure 13. Excitation with 395 nm wavelength resulted in reddish-orange emission in case of all samples. Silver amount did not influence the emission color significantly. For simplicity, only samples annealed for 6 hours are presented since all obtained samples emitted similar red to orange color.

4. Conclusions

Presented XRD results have shown that amorphous material of $73TeO_2$-4BaO-$3Bi_2O_3$-$2Eu_2O_3$-xAg (where $x = 1$, 2, and 3) composition has been successfully obtained. No crystallization of glass matrix is detected in the as-prepared samples due to correct conditions of melt-quenching process. DSC study revealed that glass transition temperature and thermal stability TS changes only slightly with introduction of silver ions. For TeO_2-BaO-Bi_2O_3 glass matrix and TeO_2-BaO-Bi_2O_3-Ag sample T_g was determined as 321 and 318°C, respectively. Thermal stability parameter was slightly decreased after silver addition. This is caused by introduction of some nonbridging oxygen in glass matrix which would lead to slight decrease of glass transition temperature. Thus, obtained material is considered to be thermally stable. FTIR results presented that after exposure to heat treatment for excessive time ratio of signal intensities due to TeO_3 and TeO_4 species does not change significantly. This in fact confirms that glass matrix is not influenced by HT process and its structure is heat resistant. XPS measurement indicated that in case of Ag1 and Ag3 glass samples annealed for 6 hours most of silver changed its valance state to Ag^0. Shape, position, and distance between Ag3d doublet also corresponds to metallic silver. Highest amount of Ag^0 has been determined in case of Ag3 series probably due to higher silver content. With the employment of TEM imaging technique, round-shaped silver nanoparticles have been observed in case of samples with different silver content and heat treatment time. More importantly, silver nanoparticles increase their sizes with increasing silver content. Nanoparticles diameters were in the range of 20–50 nm. UV-vis absorption results additionally proved that silver nanoparticles have been obtained. It is concluded that change of the silver content together with modification of heat treatment time can result in tunable LSPR band and silver nanoparticles dimensions. It is promising to further study the influence of HT process on silver nanoparticles properties. Photoluminescence measurements presented the enhancement of Eu^{3+} emission bands in case of AgEu1 sample. Enhancement is observed until 6 hours of annealing is applied. Then, for 12 and 24 hours of heat treatment, decrease of intensity is observed probably due to Eu^{3+}-AgNP energy transfer. Obtained materials could find application in tunable red to yellow-white light emitters.

Conflicts of Interest

The authors declare that they have no conflicts of interest.

References

[1] Y. Cheng, Z. Wu, X. Hu, T. Wu, and W. Zhou, "Thermal stability and optical properties of a novel Tm3+ doped fluorotellurite glass," *Journal of Rare Earths*, vol. 32, no. 12, pp. 1154–1161, 2014.

[2] H. Lin, S. Tanabe, L. Lin et al., "Infrequent blue and green emission transitions from Eu3+ in heavy metal tellurite glasses with low phonon energy," *Physics Letters A*, vol. 358, no. 5-6, pp. 474–477, 2006.

[3] Y. Gao, Q.-H. Nie, T.-F. Xu, and X. Shen, "Study of luminescence properties of novel Er3+ single-doped and Er3+/Yb3+ co-doped tellurite glasses," *Spectrochimica Acta Part A: Molecular and Biomolecular Spectroscopy*, vol. 61, no. 6, pp. 1259–1262, 2005.

[4] E. A. Lalla, U. R. Rodríguez-Mendoza, A. D. Lozano-Gorrín, A. Sanz-Arranz, F. Rull, and V. Lavín, "Nd3+-doped TeO2-PbF2-AlF3 glasses for laser applications," *Optical Materials*, vol. 51, pp. 35–41, 2016.

[5] Y. Lu, M. Cai, R. Cao, S. Qian, S. Xu, and J. Zhang, "Er3+ doped germanate-tellurite glass for mid-infrared 2.7μm fiber laser material," *Journal of Quantitative Spectroscopy & Radiative Transfer*, vol. 171, pp. 73–81, 2016.

[6] X. Pi, X. Cao, Z. Fu et al., "Application of Te-Based Glass in Silicon Solar Cells," *Acta Metallurgica Sinica (English Letters)*, vol. 28, no. 2, pp. 223–229, 2015.

[7] D. Li, W. Xu, P. Kuan et al., "Spectroscopic and laser properties of Ho3+ doped lanthanum-tungsten-tellurite glass and fiber," *Ceramics International*, vol. 42, no. 8, pp. 10493–10497, 2016.

[8] A. Maaoui, F. Ben Slimen, M. Haouari, A. Bulou, B. Boulard, and H. Ben Ouada, "Upconversion and near infrared emission properties of a novel Er3+/Yb3+ codoped fluoro-tellurite glass," *Journal of Alloys and Compounds*, vol. 682, pp. 115–123, 2016.

[9] V. A. G. Rivera, Y. Ledemi, S. P. A. Osorio et al., "Efficient plasmonic coupling between Er3 +:(Ag/Au) in tellurite glasses," *Journal of Non-Crystalline Solids*, vol. 358, no. 2, pp. 399–405, 2012.

[10] I. Soltani, S. Hraiech, K. Horchani-Naifer, H. Elhouichet, B. Gelloz, and M. Férid, "Growth of silver nanoparticles stimulate spectroscopic properties of Er3+ doped phosphate glasses: Heat treatment effect," *Journal of Alloys and Compounds*, vol. 686, pp. 556–563, 2016.

[11] O. L. Malta, P. A. Santa-Cruz, G. F. De Sá, and F. Auzel, "Fluorescence enhancement induced by the presence of small silver particles in Eu3+ doped materials," *Journal of Luminescence*, vol. 33, no. 3, pp. 261–272, 1985.

[12] M. E. Camilo, T. A. A. Assumpção, D. M. Da Silva, D. S. Da Silva, L. R. P. Kassab, and C. B. De Araújo, "Influence of silver nanoparticles on the infrared-to-visible frequency upconversion in Tm3/Er3/Yb3 doped GeO 2-PbO glass," *Journal of Applied Physics*, vol. 113, no. 15, Article ID 153507, 2013.

[13] H.-R. Bahari, R. Zamiri, H. A. A. Sidek, A. Zakaria, and F. R. M. Adikan, "Characterization and synthesis of silver nanostructures in rare earth activated GeO2-PbO glass matrix using matrix adjustment thermal reduction method," *Entropy*, vol. 15, no. 5, pp. 1528–1539, 2013.

[14] Y. Hu, J. Qiu, Z. Song et al., "Spectroscopic properties of Tm3+/Er3+/Yb3+ co-doped oxyfluorogermanate glasses containing silver nanoparticles," *Journal of Luminescence*, vol. 145, pp. 512–517, 2014.

[15] S. Mohapatra, "Tunable surface plasmon resonance of silver nanoclusters in ion exchanged soda lime glass," *Journal of Alloys and Compounds*, vol. 598, pp. 11–15, 2014.

[16] V. A. G. Rivera, D. Manzani, Y. Messaddeq, L. A. O. Nunes, and E. Marega Jr., "Study of Er3+ fluorescence on tellurite glasses containing Ag nanoparticles," *Journal of Physics: Conference Series*, vol. 274, no. 1, Article ID 012123, 2011.

[17] Q. Jiao, X. Wang, J. Qiu, and D. Zhou, "Effect of silver ions and clusters on the luminescence properties of Eu-doped borate glasses," *Materials Research Bulletin*, vol. 72, pp. 264–268, 2015.

[18] S. Fan, C. Yu, D. He, K. Li, and L. Hu, "White light emission from γ-irradiated Ag/Eu co-doped phosphate glass under NUV light excitation," *Journal of Alloys and Compounds*, vol. 518, pp. 80–85, 2012.

[19] R. J. Amjad, M. R. Dousti, M. R. Sahar et al., "Silver nanoparticles enhanced luminescence of Eu3+-doped tellurite glass," *Journal of Luminescence*, vol. 154, pp. 316–321, 2014.

[20] M. R. Dousti, M. R. Sahar, M. S. Rohani et al., "Nano-silver enhanced luminescence of Eu^{3+}-doped lead tellurite glass," *Journal of Molecular Structure*, vol. 1065-1066, no. 1, pp. 39–42, 2014.

[21] Y. Y. Du, B. J. Chen, E. Y. B. Pun, Z. Q. Wang, X. Zhao, and H. Lin, "Silver nanoparticles enhanced multichannel transition luminescence of Pr3+ in heavy metal germanium tellurite glasses," *Optics Communications*, vol. 334, pp. 203–207, 2015.

[22] H. Fares, H. Elhouichet, B. Gelloz, and M. Férid, "Silver nanoparticles enhanced luminescence properties of Er3+ doped tellurite glasses: Effect of heat treatment," *Journal of Applied Physics*, vol. 116, no. 12, Article ID 123504, 2014.

[23] B. Huang, Y. Zhou, P. Cheng, Z. Zhou, J. Li, and G. Yang, "The 1.85 μm spectroscopic properties of Er3+/Tm3+co-doped tellurite glasses containing silver nanoparticles," *Journal of Alloys and Compounds*, vol. 686, pp. 785–792, 2016.

[24] L. Wu, Y. Zhou, Z. Zhou et al., "Effect of silver nanoparticles on the 1.53 μm fluorescence in Er3+/Yb3+ codoped tellurite glasses," *Optical Materials*, vol. 57, pp. 185–192, 2016.

[25] G. Laudisio and M. Catauro, "Glass transition temperature and devitrification behaviour of glasses in the Na2O·4GeO2-K2O·4GeO2 composition range," *Materials Chemistry and Physics*, vol. 51, no. 1, pp. 54–58, 1997.

[26] M. Ramstedt and P. Franklyn, "Difficulties in determining valence for Ag0 nanoparticles using XPS - Characterization of nanoparticles inside poly (3-sulphopropyl methacrylate) brushes," *Surface and Interface Analysis*, vol. 42, no. 6-7, pp. 855–858, 2010.

[27] K. Sadecka, M. Gajc, K. Orlinski et al., "When eutectics meet plasmonics: Nanoplasmonic, volumetric, self-organized, silver-based eutectic," *Advanced Optical Materials*, vol. 3, no. 3, pp. 381–389, 2015.

[28] A. Dietzel, "Glass structure and glass properties," *Glastechnische Berichte-Glass Science and Technology*, vol. 22, pp. 41–45, 1968.

[29] E. Culea, I. Vida-Simiti, G. Borodi, E. N. Culea, R. Stefan, and P. Pascuta, "Effects of Er^{3+}:Ag codoping on structural and spectroscopic properties of lead tellurite glass ceramics," *Ceramics International*, vol. 40, no. 7, pp. 11001–11007, 2014.

[30] N. M. Yusoff and M. R. Sahar, "The incorporation of silver nanoparticles in samarium doped magnesium tellurite glass: Effect on the characteristic of bonding and local structure," *Physica B: Condensed Matter*, vol. 470-471, pp. 6–14, 2015.

[31] M. Walas, A. Pastwa, T. Lewandowski et al., "Luminescent properties of Ln3+ doped tellurite glasses containing AlF3," *Optical Materials*, vol. 59, pp. 70–75, 2016.

[32] P. Prieto, V. Nistor, K. Nouneh, M. Oyama, M. Abd-Lefdil, and R. Díaz, "XPS study of silver, nickel and bimetallic silver-nickel nanoparticles prepared by seed-mediated growth," *Applied Surface Science*, vol. 258, no. 22, pp. 8807–8813, 2012.

[33] A. Dehelean, S. Rada, I. Kacso, and E. Culea, "IR, UV-vis spectroscopic and DSC investigations of europium doped

tellurite glasses obtained by sol-gel synthesis," *Journal of Physics and Chemistry of Solids*, vol. 74, no. 9, pp. 1235–1239, 2013.

[34] Y. Wu, X. Shen, S. Dai et al., "Silver nanoparticles enhanced upconversion luminescence in Er 3+/Yb 3+ codoped bismuth-germanate glasses," *The Journal of Physical Chemistry C*, vol. 115, no. 50, pp. 25040–25045, 2011.

[35] A. N. Goldstein, *Handbook of Nanophase Materials*, CRC Press, 1997.

[36] Y. Qi, Y. Zhou, L. Wu et al., "Silver nanoparticles enhanced 1.53 μm band fluorescence of Er 3+/Yb3+ codoped tellurite glasses," *Journal of Luminescence*, vol. 153, pp. 401–407, 2014.

[37] W. Stambouli, H. Elhouichet, B. Gelloz, and M. Férid, "Optical and spectroscopic properties of Eu-doped tellurite glasses and glass ceramics," *Journal of Luminescence*, vol. 138, pp. 201–208, 2013.

[38] W. A. Pisarski, L. Zur, M. Kowal, and J. Pisarska, "Enhancement and quenching photoluminescence effects for rare earth - Doped lead bismuth gallate glasses," *Journal of Alloys and Compounds*, vol. 651, pp. 565–570, 2015.

[39] K. Binnemans, "Interpretation of europium(III) spectra," *Coordination Chemistry Reviews*, vol. 295, pp. 1–45, 2015.

[40] A. Dwivedi, C. Joshi, and S. B. Rai, "Effect of heat treatment on structural, thermal and optical properties of Eu^{3+} doped tellurite glass: formation of glass-ceramic and ceramics," *Optical Materials*, vol. 45, pp. 202–208, 2015.

[41] C. B. De Araujo, D. Silvério Da Silva, T. A. Alves De Assumpção, L. R. P. Kassab, and D. Mariano Da Silva, "Enhanced optical properties of germanate and tellurite glasses containing metal or semiconductor nanoparticles," *The Scientific World Journal*, vol. 2013, Article ID 385193, 2013.

[42] M. Reza Dousti and S. Raheleh Hosseinian, "Enhanced upconversion emission of Dy^{3+}-doped tellurite glass by heat-treated silver nanoparticles," *Journal of Luminescence*, vol. 154, pp. 218–223, 2014.

[43] J. N. Farahani, D. W. Pohl, H.-J. Eisler, and B. Hecht, "Single quantum dot coupled to a scanning optical antenna: a tunable superemitter," *Physical Review Letters*, vol. 95, no. 1, Article ID 017402, 2005.

[44] A. Chiasera, M. Ferrari, M. Mattarelli et al., "Assessment of spectroscopic properties of erbium ions in a soda-lime silicate glass after silver-sodium exchange," *Optical Materials*, vol. 27, no. 11, pp. 1743–1747, 2005.

[45] H. Mertens, A. F. Koenderink, and A. Polman, "Plasmon-enhanced luminescence near noble-metal nanospheres: Comparison of exact theory and an improved Gersten and Nitzan model," *Physical Review B: Condensed Matter and Materials Physics*, vol. 76, no. 11, Article ID 115123, 2007.